

# Advances in meso-mechanical analysis of concrete specimens using zero-thickness interface elements

I. Carol, A. Idiart & C.M. Lopez

*School of Civil Engineering (ETSECCPB) – Technical University of Catalonia (UPC), Barcelona, Spain*

A. Caballero

*School of Civil & Resource Engineering, Univ. of Western Australia, Perth.*

**ABSTRACT:** Mesomechanical analysis is emerging as a powerful tool for the modeling of material behavior. The group of mechanics of materials at ETSECCPB has been developing such tools for concrete, with the distinctive feature of the way of representing a key ingredient of concrete behavior, cracking. All lines in the FE mesh are considered as potential crack lines and, for them, traction-separation constitutive models based on principles of non-linear fracture mechanics have been developed and implemented. This approach has been implemented in the context of the FEM, originally in 2D and more recently in 3D, *via* systematic use of zero-thickness interface elements. The geometry of the particles (larger aggregates) is generated numerically using Delaunai/Voronoi theory, shrunk to allow space for mortar, and finally the overall specimen is “cut” to its final shape. Results of mechanical analysis turn out very realistic, both mesoscopically (distributed microcrack, coalescence, localization) and macroscopically (average stress-strain curves for specimen). Ongoing work aims at more complex geometries and loading cases, more efficient computational methods and to extension to diffusion-dominated and coupled phenomena such as environmental deterioration or high temperatures.

## 1 INTRODUCTION

Since the pioneering *numerical concrete* of Roelfstra et al. (1985), it has become progressively clearer that mesomechanical analysis is a powerful approach to predict complex material behavior starting from relatively simple assumptions. The price to pay, however, is high computational cost associated to modeling explicitly the first-level heterogeneities of the material, in the case of concrete normally the larger aggregate pieces floating on a mortar matrix. Since then, a certain number of such models have been already proposed, first in 2D, more recently in 3D, some based on particle representations of the “DEM”-type or associated truss or beam structures between particle centers (Vonk 1992; Cusatis et al. 2003a, 2003b; Bolander & Saito 1998; Bolander et al. 2000), some based on the regular lattice concept (Schlangen & van Mier 1993; Lilliu & van Mier 2003), and some on the classical continuum-type (Stankowski 1990; Wang & Huet 1993). In all them a key factor is how to represent cracking. In the first and second type (particles, lattices), cracking may be identified *a posteriori* as adjacent adequately aligned failed beam or truss elements. This leads apparently meaningful cracks, but makes it difficult to verify concepts such as fracture energy, size effect, etc. In the third type (continuum), cracks may be represented either via smeared (e.g. Stankowski 1990) or

discrete approach (e.g. Wang & Huet 1993). The smeared approach leads to some well-known problems such as inobjectivity with mesh size or limited deformation modes of the standard continuum elements, which have led to a variety of techniques for regularization, crack tracking, etc. but no universal method in sight yet for handling a general cracking problem. The discrete approach avoids the above difficulties, but generates others. Except for the simplified case of crack path known *a priori* (e.g. 3-point bending beam) the general implementation of the discrete approach with traveling crack tips requires intensive remeshing (e.g. Ingraffea & Saouma 1985) and exhibits unresolved challenges, being limited in practice to one or two (or very few) simultaneous cracks. An alternative approach, already mentioned in Rots (1988) consists of considering each line of the mesh as a potential crack, insert zero-thickness interface elements equipped with a fracture-based constitutive law, and let them open, close and reopen depending on local stress evolution. This is the approach followed in this paper.

In subsequent sections, the work for concrete developed by the authors during the last decade, first in 2D, then in 3D and also incorporating other effects such as time-dependent, diffusion-driven and durability-related phenomena, is described. The paper is concluded with some remarks on the approach fol-

lowed and a brief description of related on-going work in the group.

## 2 ORIGINAL 2D MESOMECHANICAL MODEL

The model originally developed for the analysis of concrete specimens in 2D, described in detail in Lopez (1999) and Carol et al. (2001) is only briefly summarized here. Following previous work by Stankowski (1990), the particle geometry was generated using Delaunai/Voronoi polygons which were then shrunk, and the space left between particles was considered filled by a matrix formed by mortar plus the smaller aggregates. Both phases were discretized using standard triangular continuum elements. A sample mesh of this type is depicted in Fig. 1, with separate representation of the mortar matrix (Fig. 1a) and aggregate particles (Fig. 1b)

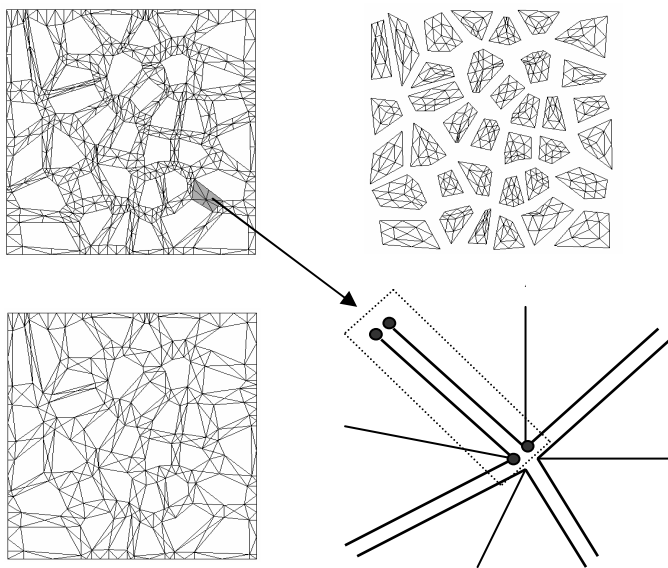


Figure 1. FE discretization of the 6x6 arrangement: a) matrix, b) aggregates, c) interfaces inserted, and d) details of discretization.

The possibility of cracking is introduced via zero-thickness interface elements with double nodes (Fig. 1d), which are inserted along all the lines of the mesh which are considered as potential crack lines. In the examples of the figure, these are all aggregate-matrix contacts plus a number of lines connecting aggregates through the matrix, which are laid out following the proposal in Vonk (1992) (Fig. 1c).

For the original calculations, the continuum elements were assumed linear elastic, and all the nonlinearities were concentrated in the interface elements, for which a traction-separation constitutive model based on non-linear fracture mechanics concepts was developed (Carol et al. 1997). That model has elasto-plastic structure, a three-parameter hyperbolic initial failure (cracking) surface, and softening evolution laws based on the accumulated energy spent on the fracture process, which is evaluated as plastic dissipation minus frictional work.

With this model, very promising results were obtained even using relatively crude meshes. Cases analyzed ranged from uniaxial tension, uniaxial compression and biaxial tension-compression, to Brazilian, and other more complex loading cases and effects. All of them gave realistic results in terms of both microcrack pattern and evolution, and macroscopic average stress-average strain curves. In particular, Fig. 2 includes resulting crack patterns for uniaxial tension along the x-axis (Fig. 2-left) and for a Brazilian test with load applied on small central sections of upper and lower faces (Fig. 2-right).

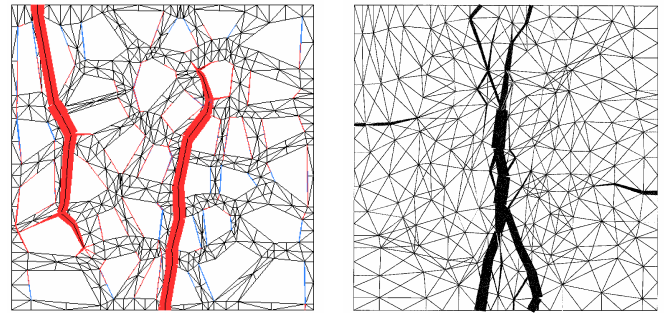


Figure 2. Crack patterns obtained in two examples of application: uniaxial tension along x-axis (left) and Brazilian test with load applied on small central sections of upper and lower faces (right).

More details about these and other application examples of mechanical behavior in 2D can be found in Lopez (1999); Lopez et al. (2000); Carol et al. (2001).

The original 2D mesomechanical model was additionally extended to represent other aspects of concrete and other materials such as:

- High-strength or light-weight aggregate concrete, in which mortar has comparable or higher mechanical properties than aggregates: In this case, adequate discretization and systematic use of interface elements were also employed within the aggregates, with interface properties adequately chosen. In this way, depending on properties and loading, cracks could also develop through aggregates, leading in that case to higher overall brittleness (Lopez 1999).
- Basic creep behavior of concrete. Mortar was assumed visco-elastic: Under constant stress this would lead to time-dependent strain increments (creep) and also stress redistribution due to time-independent aggregates. The latter effect lead to non-linear creep and also to failure under sustained load, with qualitatively correct Rush curves (Lopez et al. 2001).
- Effect of specimen height and verification of fracture energy concept (Ciancio et al. 2002; Lopez et al. 2004): Rectangular specimens of various height-to-width ratios were analyzed

under uniaxial tension and uniaxial compression, in order to reproduce the experimental results reported in van Mier (1997), in which the various overall stress-strain curves may look quite different after the peak, while they are much more coincident in terms of stress-post-peak displacement.

- Other materials: applications of the same meso-mechanical model with zero-thickness fracture-based interfaces were developed for porous sandstone rock and for cellular materials such as trabecular bone tissue. In the former case the motivating problem is sand production in oil reservoirs (Garolera et al. 2005), and in the second inelastic behavior of that porous biological material, with special emphasis on anisotropy (Roa et al. 2000; Carol et al. 2001; Roa 2004).

### 3 EXTENSION TO 3D

In a second stage of development the meso-mechanical model has been extended to 3D. Although between 2D and 3D the concepts do not change much, this extension has required very significant efforts and new non-trivial developments in all fronts of activity, i.e. geometry and mesh generation, constitutive model, computational efficiency, graphic representation, etc. All these developments, together with some numerical results are summarized in this section. More details can be found in Caballero (2005); Caballero et al. (2006a, 2006b); Caballero et al. (2007).

#### 3.1 Geometry and meshes

The procedure for particle geometry and mesh generation in 3D is schematized in Fig. 3 in the next page. The departing point is a regular distribution of points (Fig. 3c), arranged according to the “Body Centered Cube” (BCC) distribution (Fig. 3a), which leads to basic 14-side polyhedra (Fig. 3b) and exhibits advantages in front of alternative possibilities (Okabe et al. 1992). The position of the initial points is randomly perturbed (Fig. 3d), and on them a Delaunay mesh of tetrahedra is generated (Fig. 3e). The dual Voronoi polygons are then shrunk (Fig. 3f), the space in between filled with matrix blocks (Fig. 3g) and the specimen sides “cut” to obtain flat surfaces (Fig. 3h). A first correction step of resulting ill-conditioned blocks (too flat or needle-type) is followed by the insertion of interface planes along the aggregate-mortar interface (Fig. 3k) and also across the mortar itself (Fig. 3l,m), in such way that the main potential fracture surfaces around and between aggregates are represented. A second check and correction of potentially ill-conditioned blocks is performed, before the FE meshing of the continuum elements, which simply consists in a subdivision of

each tetrahedral block in a fixed number of tetrahedral finite elements. Finally, the interface elements are introduced along all potential fracture planes already present in the FE mesh, which basically consists of an orderly duplication of the nodes and subsequent changes in element nodal connectivities. This process increases the number of nodes considerably while the number of continuum elements remains unchanged.

#### 3.2 Constitutive model

The interface constitutive formulation in 3D (Caballero, 2006) is an extension of the previous 2D model. Interface behavior is formulated in terms of one normal and two tangential traction components on the plane of the joint,  $\sigma = [\sigma_N, \sigma_{T1}, \sigma_{T2}]^t$  and the corresponding relative displacements  $u = [u_N, u_{T1}, u_{T2}]^t$ . The model has the structure of work-softening elasto-plasticity, in which plastic relative displacements can be identified with crack openings and normal and shear elastic stiffness  $K_N, K_T$  play the role of penalty coefficients, i.e. they are set to very high values to minimize the subsequent elastic deformations. The initial loading (failure) surface  $F = 0$  is given as a three-parameter hyperboloid with tensile strength  $\chi$ , asymptotic “cohesion”  $c$ , and asymptotic friction angle  $\tan\phi$ .

$$F = \sigma_{T1}^2 + \sigma_{T2}^2 - (c - \sigma_N \tan\phi)^2 + (c - \chi \tan\phi)^2 \quad (1)$$

When cracking starts, the loading surface begins to shrink (softening), Fig. 4, thanks to the dependency of the surface parameters on  $W^{cr}$ , work spent in fracture processes. These softening functions incorporate the classical fracture energy in Mode I,  $G_F^I$  and a second energy under “Mode IIa” defined under shear and high compression,  $G_F^{IIa}$ , with values generally higher than its mode I counterpart. Under mode I the cracking surface shrinks and moves its vertex to the coordinate origin (no tensile stresses). Under mixed-mode, it degenerates further, asymptotically becoming a cone that represents the residual friction after all roughness of the crack surface would have been eliminated.

#### 3.3 Computational and graphics aspects

The new 3D formulation has been implemented into the existing, in-house developed FE code, DRAC (Prat et al. 1993). The implementation uses a sub-stepping technique combined with consistent tangent operator based on backward Euler method (Caballero 2005). The FE code itself has also needed considerable improvement in order to solve the resulting large systems in reasonable times.

New iterative solvers with partial factorization have been implemented. A Line-Search strategy combined with quadratic Arc-Length constitutes the iterative procedure for non-linear calculations at the

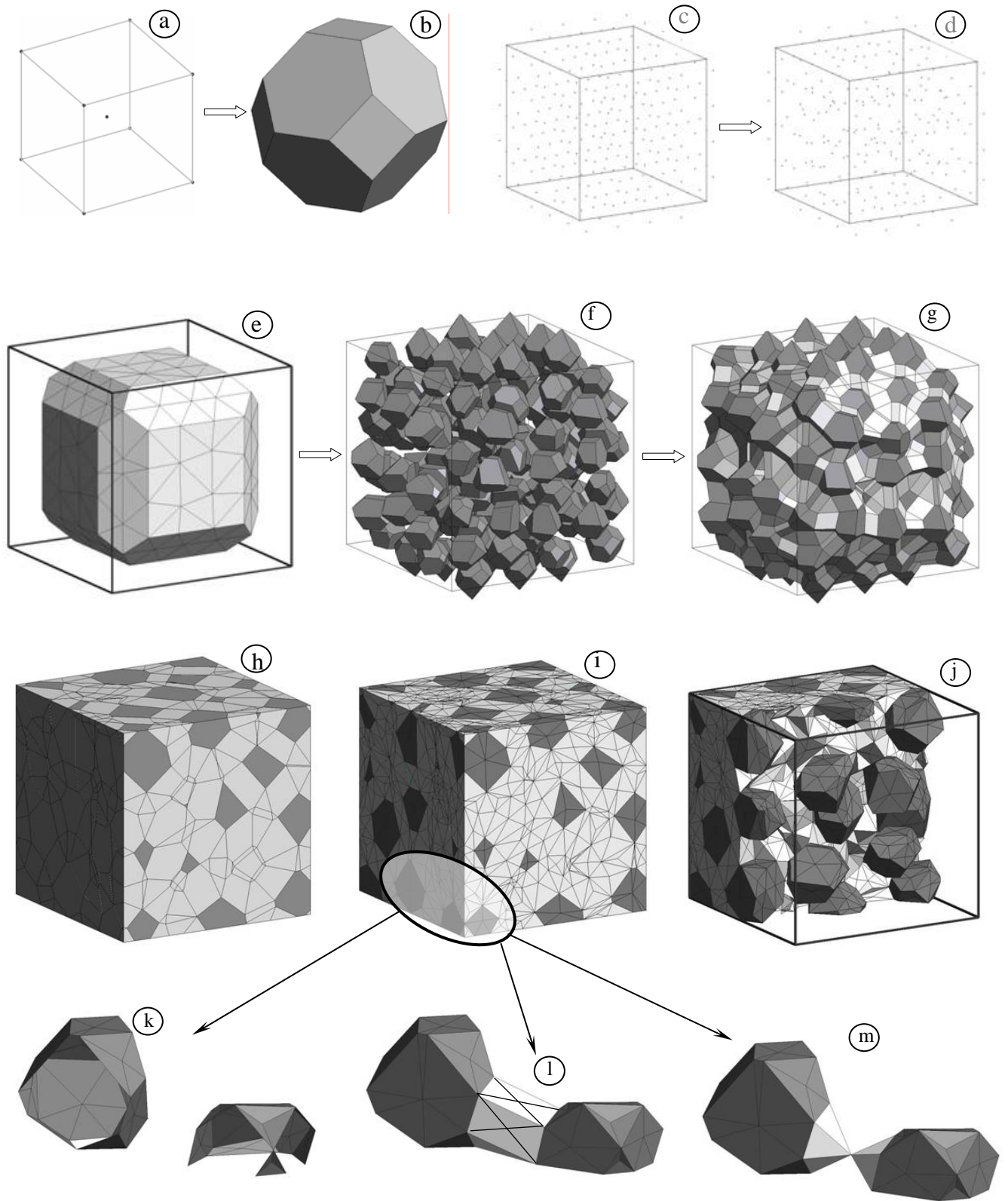


Figure 3. Meso-structural generation: a) Undistorted single BCC cell b) BCC polyhedron obtained from the undistorted BCC distribution of points c) regular distribution of points (BCC distribution) d) distorted distribution of points e) Delaunay mesh obtained from distorted distribution of points in the volume interior f) Resulting Voronoi polyhedra (aggregates) g) filling up space in between the polyhedra (mortar) h) cutting process i&j) mesh generation and interface element insertion k) aggregate-mortar interfaces l&m) mortar-mortar interfaces.

structural level. Graphic representation in 3D needed at the pre- and post-processing stages has been handled with GiD (Ribó & Riera 1997), for which adequate interfaces have been developed with FE code DRAC.

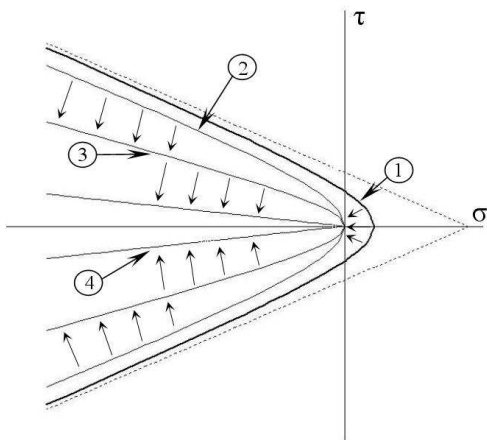


Figure 4. Interface constitutive law: evolution of fracture surface.

### 3.4 Examples

The 3D examples consist of cubical specimens of  $4 \times 4 \times 4 \text{ cm}^3$  subject to three different loading cases. The specimen contains 14 aggregate pieces with a volume fraction of 25%, and the resulting FE mesh contains 6254 nodes, 5755 tetrahedra and 3991 interface elements. The material parameters used are:  $E=70000 \text{ MPa}$  (aggregate),  $E=25000 \text{ MPa}$  (mortar) and  $\nu=0.20$  (both) for the continuum elements; for the aggregate-mortar interfaces:  $K_N=K_T=10^9 \text{ MPa/m}$ ,  $\tan\phi_0=0.6$ ,  $\tan\phi_1=0.2$ ,  $\chi_0=2 \text{ MPa}$ ,  $c_0=7.0 \text{ MPa}$ ,  $G_f^I=0.03 \text{ N/mm}$ ,  $G_f^{IIa}=10G_f^I$ ; for the mortar-mortar interfaces the same parameters except for  $\chi_0=4 \text{ MPa}$ ,  $c_0=14.0 \text{ MPa}$ ,  $G_f^I=0.06 \text{ N/mm}$ .

Uniaxial loading is applied via prescribed displacements along the desired axis for the corresponding face nodes, while lateral displacements are left free, except for the minimum number of restrictions to avoid rigid body motions. The results of applying uniaxial tension along  $x$ ,  $y$  and  $z$ -axis are represented, in terms of average stress-strain curves, in Fig. 5. The results of the uniaxial compression loading, also along  $x$ ,  $y$  and  $z$ , are represented in Fig.6 (axial stress vs. axial strain) and Fig. 7 (axial stress vs. volumetric strain). Note the realistic shape of all the curves, especially the post-peak dilatancy in compression.

The same loading cases for the  $z$ -axis only, are also illustrated in figures 8 and 9 (in the two coming full pages), in terms of microcrack evolution and deformations.

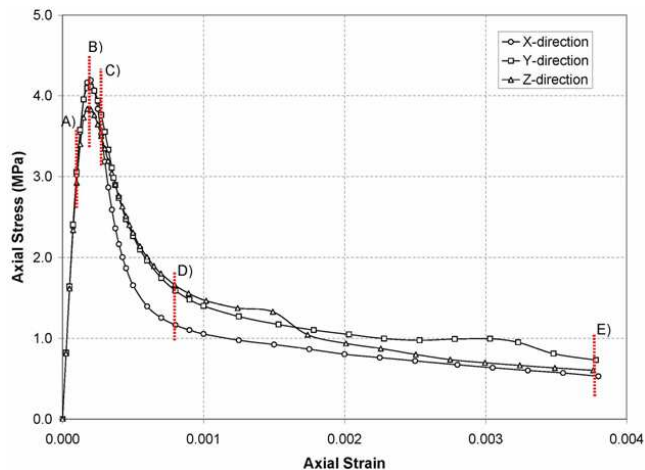


Figure 5. Stress-Strain diagram curves for the uniaxial tension test in  $x$ ,  $y$  and  $z$ .

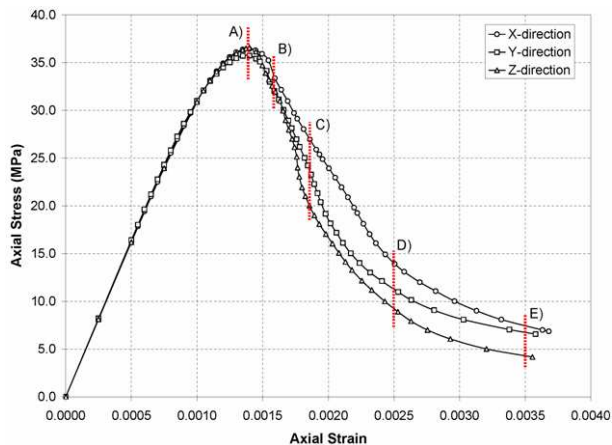


Figure 6. Stress-strain diagram curves for the uniaxial compression test in  $x$ ,  $y$  and  $z$ .

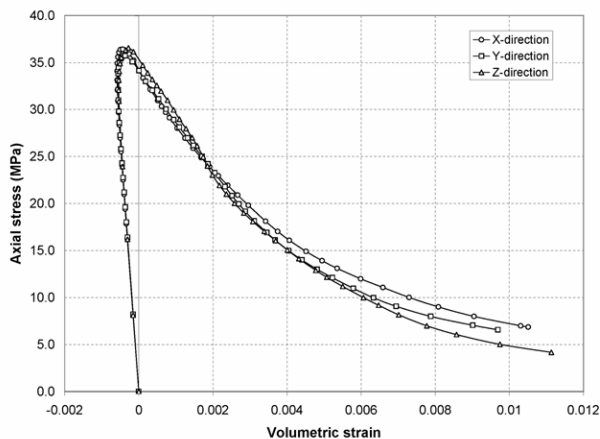


Figure 7. Stress-volumetric strain diagram curves for the uniaxial compression test in  $x$ ,  $y$  and  $z$ .

In those figures, the sequence of cracking, for the loading levels marked as A to E in figures 5 and 6, are represented. Figs. 8 and 9 are organized in a similar way, with 3 columns of 5 plots each. The left column includes those interface elements which are in plastic loading, while the middle column includes those that, after initial cracking, currently are in elastic unloading. Finally, the right column depicts the deformed mesh at each load level.

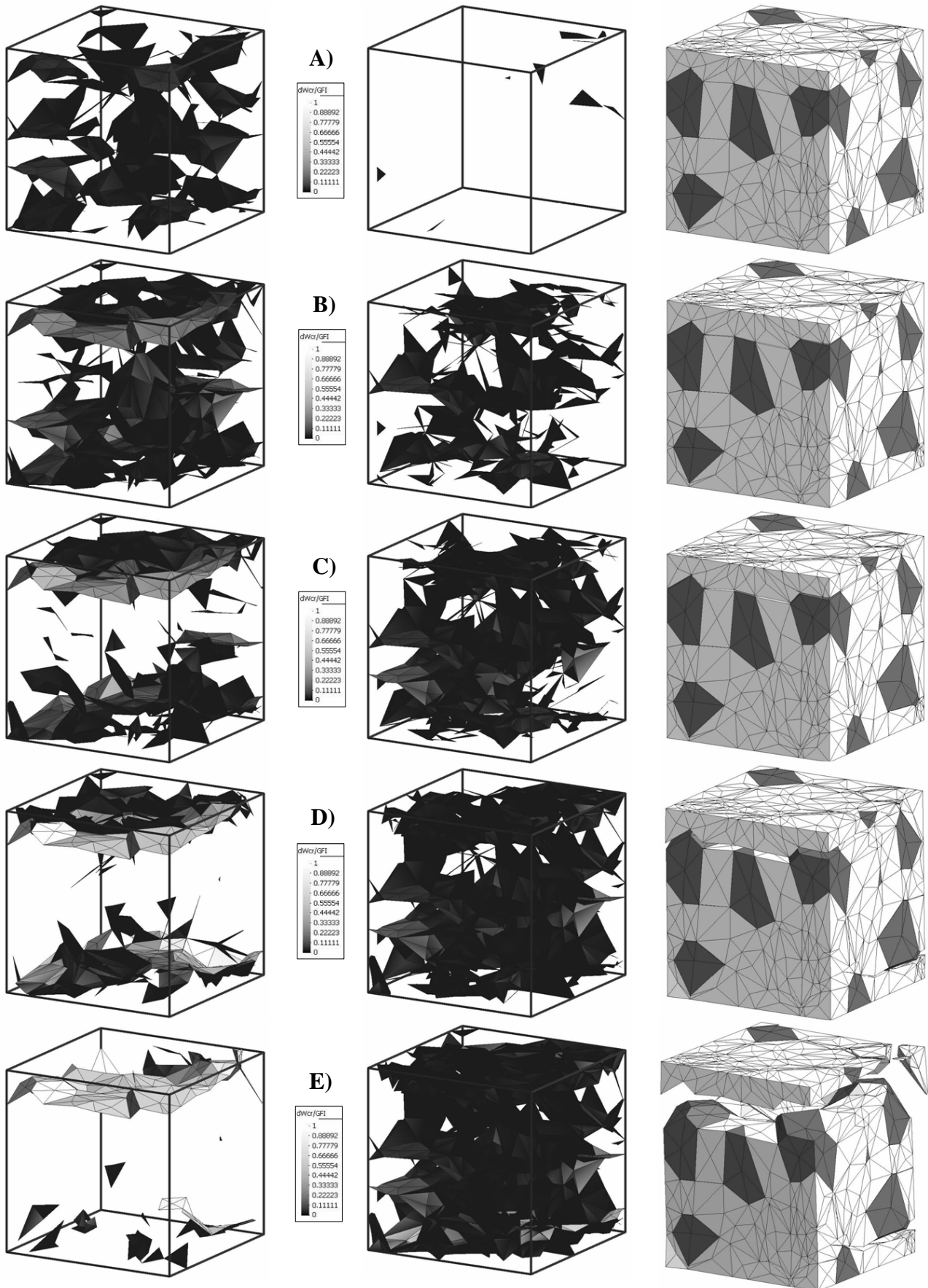


Figure 8. Results of tension test in Z direction. History parameter  $W^{cr} / G_F^I$  on opening interfaces (left column), closing interfaces (middle column), and deformed shape (right column), at loading states A, B, C, D and E.

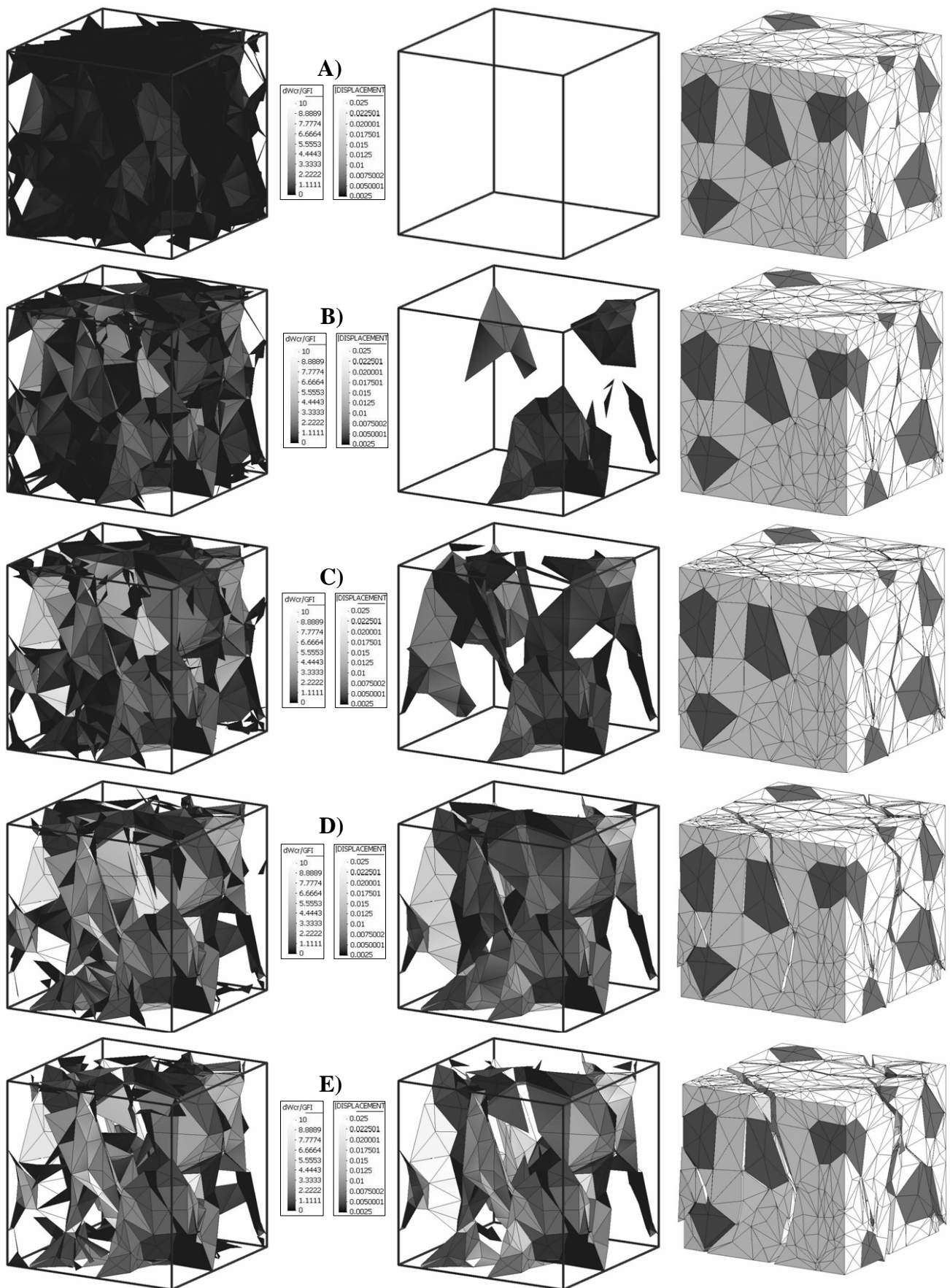


Figure 9. Results of compression test in Z direction. History parameter  $W^{cr} / GFI$  on opening interfaces (left column), norm of relative displacement on opening interfaces (middle column) and deformed shape of specimen (right column), at loading states A to E.

Note the realistic representation of micro-cracking in Figs. 8 and 9, which is widely distributed before peak, and then localizes spontaneously in only a few macro-cracks while the rest unload. More details about the results of these loading cases may be found in Caballero et al. (2006b).

The third loading case presented is biaxial loading, which is applied simultaneously along axes  $x$  and  $y$  onto the same 14-aggregate specimen, as represented in Fig 10 (view from a bottom perspective). In order to maintain fixed proportions between the  $x$  and  $y$  loads, in this case the load platens are also discretized with stiff elastic elements and interface elements in between platens and specimen.

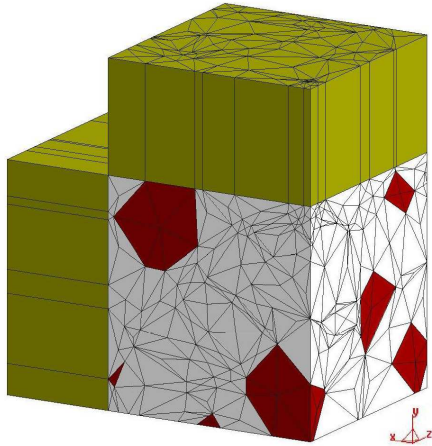


Figure 10: Finite element mesh for concrete and rigid platens used in the biaxial numerical tests.

The peak loads obtained for increasing loading and fixed  $\sigma_x/\sigma_y$  ratio, are represented in Fig. 11 in terms the angle of the path in the normalized  $\sigma_x$ - $\sigma_y$  space, showing good qualitative agreement with the classical biaxial envelope (Kupfer et al. 1969).

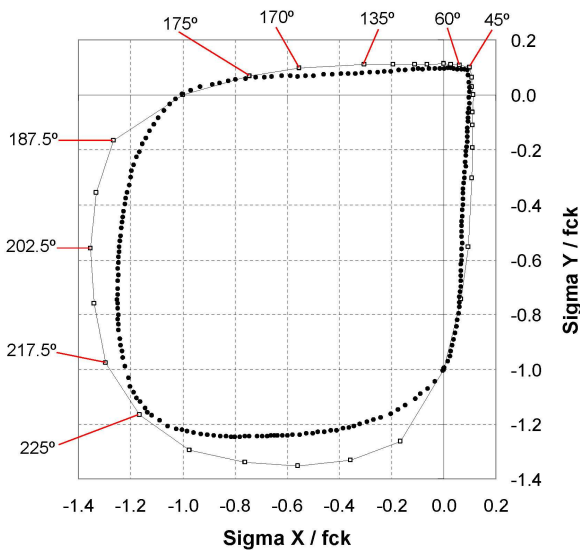


Figure 11. Comparison between experimental (marked using dots) and numerical failure envelope for biaxial loading (continuous line)

The results are also represented in terms of cracking and deformed mesh in Fig.12 (next page). In that figure, the side view of specimen from  $z$ ,  $y$  and  $x$  di-

rections are depicted in the left, central and right columns, while the two rows correspond to the cases of 60 and 225 degrees (Fig.11), (that is, to the cases of biaxial tension with  $\sigma_x = 2\sigma_y$  and equi-biaxial compression). Note that in the first case, cracks run mainly parallel to the  $z$ -axis (one can “see through” the left diagram), that is they are mostly *in-plane* cracks, while in the second they are mainly *out-of-plane* cracks (perpendicular to  $z$ , i.e. one can “see through” the right and center diagrams but not through the left one). Note that this type of effect can only be captured with a 3D model.

#### 4 EXTENSION TO DIFFUSION-DRIVEN ENVIRONMENTAL PHENOMENA

The basic 2D mesomechanical model of section 2 has also been extended in the direction of incorporating new more complex aspects of concrete behavior such as environmental-related phenomena. One of the key ingredients in that sense is moisture diffusion through the pore system, which is the main driving force inducing mechanical effects such as drying shrinkage or drying creep, and plays also a significant role in more complex conditions such as high temperature behavior and other durability-related phenomena.

##### 4.1 Drying and shrinkage at the point

Since the early work of Bazant & Najjar (1972), it is generally accepted that, at least as a first approach, moisture movements in concrete basically follow a non-linear diffusion-type equation which may be advantageously written in terms of the relative humidity at the point,  $H$  (varying between 0 and 1), as

$$\frac{\partial}{\partial x_i} \left[ D_H \frac{\partial H}{\partial x_i} \right] = \frac{\partial H}{\partial t} \quad (2)$$

where diffusivity  $D$  strongly depends on  $H$  itself. In this case, this dependency has been represented as:

$$D_H(H) = D_0 + (D_1 - D_0) f(\beta H) \quad (3)$$

in which  $D_0$  and  $D_1$  are the values for  $H=0$  and  $H=1$  respectively, and  $f$  is a transition function which depends also on a shape parameter  $\beta$ . The model also includes a “desorption isotherm”, which relates the relative humidity  $H$  to the evaporable water content in the pores  $w_e$  (e.g. grams per liter).  $w_e$  is needed for calculating the specimen weight loss, and also for predicting the “shrinkage at a point” (not same as specimen or cross-section shrinkage, which depends also on geometry, etc). In this case, the isotherm proposed by Norling (1994) is adopted. All this is represented in Fig. 13 (next page), which includes a family of diffusivity functions (left) and a typical desorption isotherm (right).

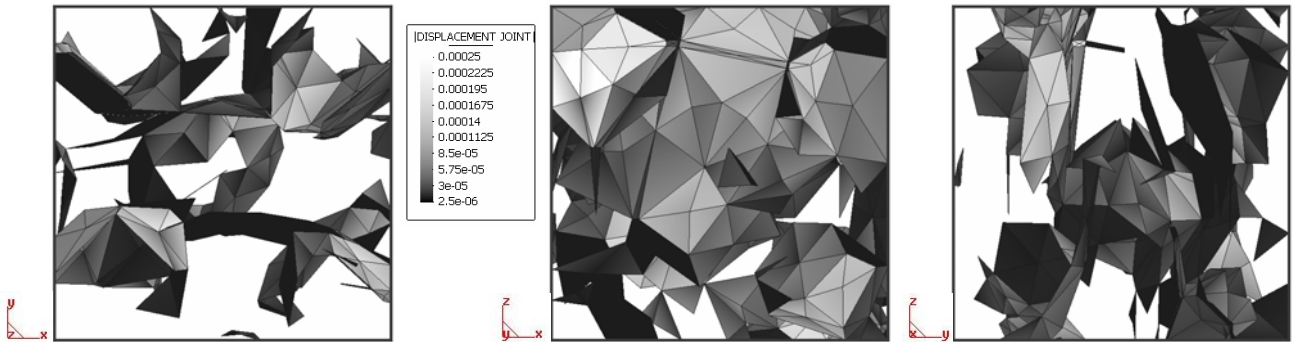


Figure 12a:  $\theta = 60^\circ$ . Cracking state in terms of relative displacement norm. Planes XY (left), XZ (center) and YZ (right).

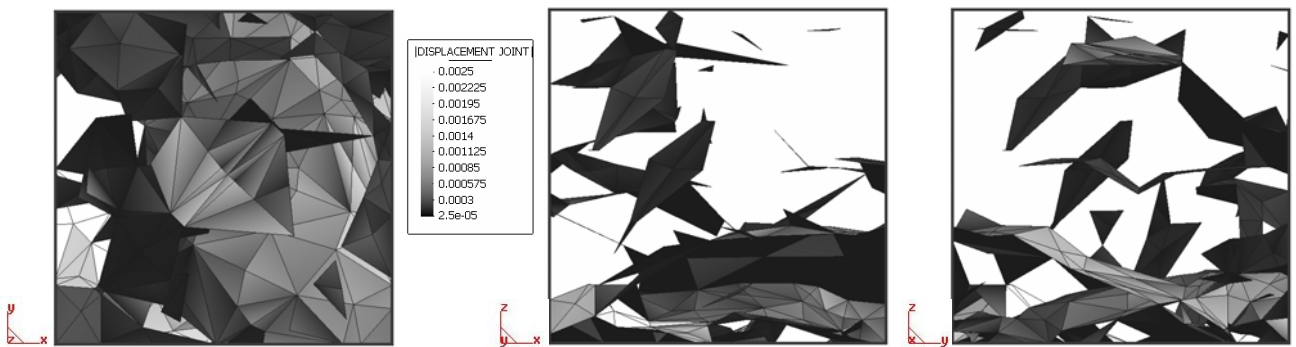


Figure 12b:  $\theta = 225^\circ$ . Cracking state in terms of relative displacement norm. Planes XY (left), XZ (center) and YZ (right).

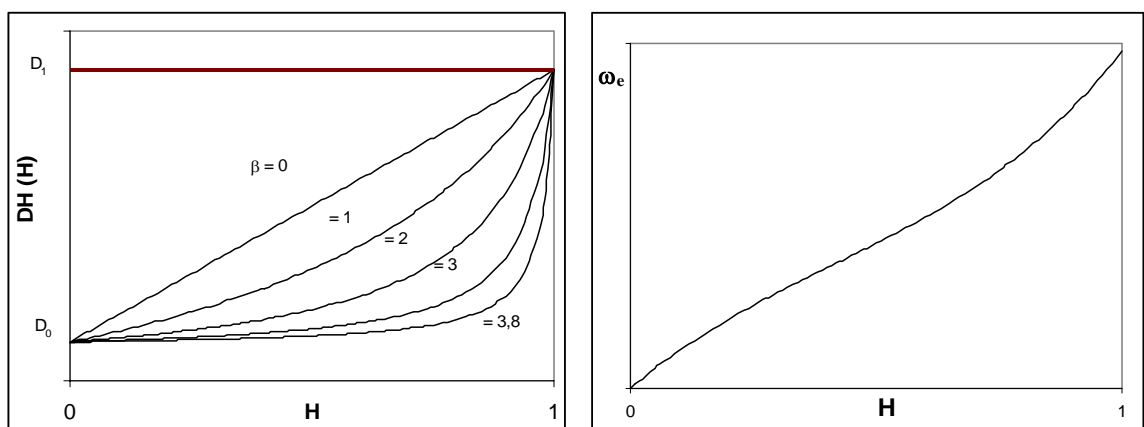


Figure 13. Diffusivity vs. Relative Humidity curve and desorption isotherm used.

Physically, it is clear that variations in moisture contents affect mechanical behavior through the material shrinkage at the point which acts similarly as a non-uniform thermal contraction, more pronounced in the parts of the specimen more exposed to drying. But also, in the opposite direction, cracks may affect diffusivity since they represent preferential channels for moisture movement. Thus, strictly speaking the phenomenon becomes fully coupled, although all seems to indicate that the second interaction is in many situations of lesser importance and in some cases may be neglected.

For the examples presented, shrinkage at the point has been assumed to be related linearly to the water loss per unit volume at each point. The material behavior for the continuum elements is assumed linear visco-elastic with aging *via* Maxwell chain representation and crack opening is assumed to increase diffusivity *via* cubic law (coupled behavior) (Lopez et al., 2005a). Under these conditions, the results presented in Fig. 14 correspond to a 6x6-aggregate square specimen subject to drying on the left and right faces (no flow is allowed through the upper and lower surfaces). Fig 14a represents the moisture distributions obtained at various drying times, with clear advancing fronts which are locally influenced by the aggregate “obstacles”. Fig. 14b represents micro-crack evolution, with initial surface cracks, which later unload while cracking develops in the interior of the specimen, in a radial configuration around aggregates, as reported from experiments (Bisschop & van Mier 2002). Finally, Fig. 14c shows the magnified deformed meshes, exhibiting the typical barrel shapes and cracks that could be intuitively expected. Additional results of shrinkage simulations w/ and w/o coupling and visco-elastic effects may be found in Lopez et al. (2005a, 2005b).

## 5 CONCLUDING REMARKS AND ON-GOING DEVELOPMENTS

The approach developed for meso-mechanical analysis of concrete and other heterogeneous quasi-brittle materials still has some limitations/drawbacks such as the high number of degrees of freedom due to node multiplication at interface intersections and the subsequent computational cost, which impose limitations on the size of the problem to be analyzed. Also, crack locations are restricted to the initial mesh lines/surfaces, which may certainly represent a source of bias on the potential crack trajectories. However, in spite of those limitations and of the relatively rudimentary geometries and specimens analyzed so far, the approach has led to very satisfactory results at meso and macro levels of observation. In particular one can highlight the realistic micro-crack patterns and evolution obtained, with localization happening spontaneously only as the result of micro/crack interaction, with their opening

and closing depending on local stress-strain conditions and the principles of mechanics exclusively (i.e. without the need of introducing any extra *ad-hoc* procedure such as tracking algorithms, etc.). Also remarkable are the overall curves in terms of average stress and strain of specimen obtained, which really capture the main well known features observed in experiments such as uniaxial compression dilatancy in the post-peak, biaxial failure envelope, creep, shrinkage, etc. Overall, this may be interpreted in the sense that the model really incorporates the essential aspects of the material behavior and, therefore, even if each ingredient is not too sophisticated, the most important observed features of concrete are already reproduced.

Current efforts in the research group, in the area of meso-mechanical analysis, are aimed at the exploitation of the models developed, at their extension to include new phenomena, and at the improvement of related numerical techniques to reduce/eliminate current drawbacks; in particular some of the on-going and planned developments are:

- exploitation of the 3D model to simulate additional experimental results such as triaxial loading under constant lateral pressure, etc, or of numerical tests difficult to carry out in the lab, such as Willam’s test under rotation of principal directions (Willam et al. 1987), etc. as well as comparison between 3D and 2D calculations, when applicable.
- exploitation of the moisture diffusion/coupled formulation to study the effect of aggregate size and volume ratio on drying shrinkage (Bisschop & van Mier 2002).
- extension of the diffusion-driven and coupled calculations to include more complex phenomena such as drying creep, durability problems involving chemistry aspects such as expansions due to sulfate-attack, or high-temperature behavior including water phase changes, etc.
- development of new fully coupled T-H-M-C code which overcomes the limitations of staggered approach followed for the first coupled calculations already performed.
- application of the approach to materials other than concrete; in particular completion of the on-going study on sand production in oil wells involving sandstone rock, and of previous studies on cellular materials with application to trabecular bone.
- development of new analysis procedures to avoid systematic node duplication due to the use of interface elements from the beginning of the analysis. Work already accomplished along this line includes new methods for evaluation of stress-tractions across mesh lines w/o interfaces emanating from a nodal point and cracking conditions at such nodal points, among others (Ciancio et al. (2006, 2007).

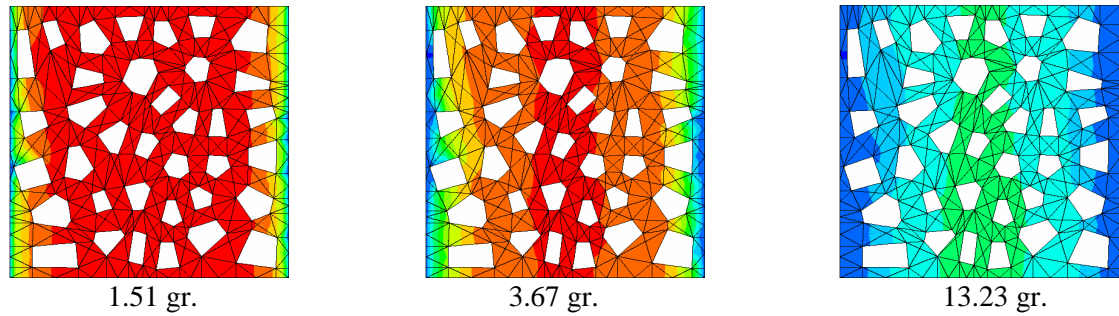


Figure 14a. Distributions of relative humidity and weight loss after 20, 200 and 10.000 days.

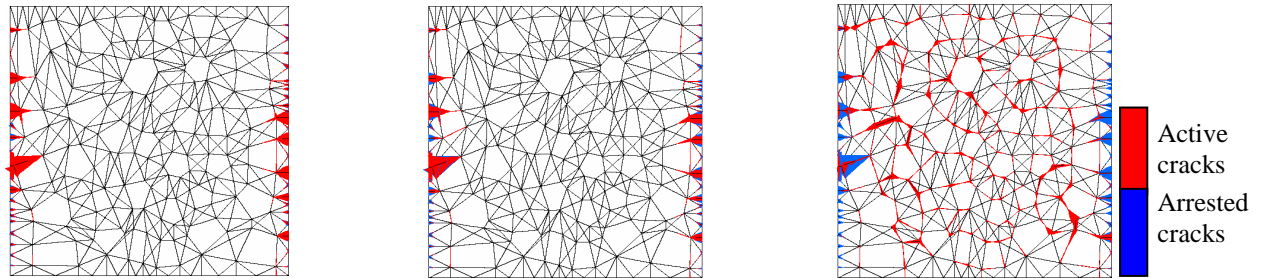


Figure 14b. Fracture energy dissipated  $W^{cf}$  in cracked interfaces after 20, 200 and 10.000 days.

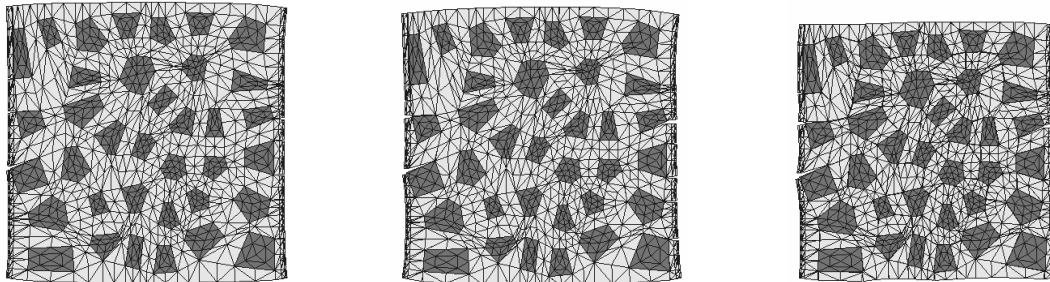


Figure 14c. Deformed meshes after 20, 200 and 10.000 days (magnification factor 150).

## ACKNOWLEDGEMENTS

This research has been supported by grants MAT2003-02481 and BIA2006-12717 funded by MEC (Madrid), and 80015/A04 funded by MFOM (Madrid). The second, third and fourth authors wish to thank MEC for the doctoral fellowships and “Ramon y Cajal” research position received during the period in which their contributions to this work were developed.

## REFERENCES

- Bazant Z.P. & Najjar, L.J. 1972. Drying of concrete as a nonlinear diffusion problem. *Cement and Concrete Research*, vol.I: 461-473.
- Bisschop, J. & van Mier, J.G.M. 2002. Effect of aggregates on drying shrinkage microcracking in cement-based composites, *Materials and Structures*, 35: 453-461.
- Bolander J.E. & Saito S. 1998. Fracture analysis using spring networks with random geometry. *Engineering Fracture Mechanics* 61(5/6): 569-591.
- Bolander J.E., Hong G.S. & Yoshitake K. 2000. Structural concrete analysis using rigid-body-spring networks. *J. Comp. Aided Civil and Infrastructure Engng.* 15: 120-133.
- Caballero, A. 2005. *3D meso-mechanical numerical analysis of concrete using interface elements*. PhD thesis, ETSECCPB-UPC, E-08034 Barcelona (Spain).
- Caballero, A., López, C.M. & Carol, I. 2006a. 3D meso-structural analysis of concrete specimens under uniaxial tension. *Computer Methods in Applied Mechanics and Engineering* 195 (52): 7182-7195.
- Caballero, A., Carol, I. & López, C.M. 2006b. A meso-level approach to the 3D numerical analysis of cracking and fracture of concrete materials. *Fatigue and Fracture of Engineering Materials and Structures* 29: 979-991.
- Caballero, A., Carol, I. & López, C.M. 2007. 3D meso-mechanical analysis of concrete specimens under biaxial loading. (Submitted).
- Carol, I., Prat, P. & López, C.M. 1997. A normal/shear cracking model. Application to discrete crack analysis. *ASCE Journal of Engineering Mechanics* 123(8): 765-773.
- Carol, I., López C.M. & Roa O. 2001. Micromechanical analysis of quasi-brittle materials using fracture-based interface elements. *Int. Journal for Numerical Methods in Engineering* 52: 193-215.
- Ciancio, D., López, C.M., Carol, I & Cuomo, M. 2002. Numerical simulation of fracture localized phenomena in concrete specimens. *Third Joint Conference of Italian Group of Computational Mechanics and Ibero-latin American Association of Computational Methods in Engineering (Gimc 2002)*.

- Ciancio, D., Carol, I. & Cuomo, M. 2006. On inter-element forces in the FEM-displacement formulation, and implications for stress recovery. *Int. J. Numer. Meth. Engng.* 66:502–528.
- Ciancio, D., Carol, I. & Cuomo, M. 2007. Crack opening conditions at ‘corner nodes’ in FE analysis with cracking along mesh lines. *Engineering Fracture Mechanics* (in press).
- Cusatis, G., Bazant, Z.P. & Cedolin, L. 2003a. Confinement-shear lattice model for concrete damage in tension and compression: I. Theory. *ASCE J. Engrg. Mech.* 129 (12): 1439-1448.
- Cusatis, G., Bazant, Z.P. & Cedolin, L. 2003b. Confinement-shear lattice model for concrete damage in tension and compression: II. Computation and validation. *ASCE J. Engrg. Mech.* 129 (12): 1449-1458.
- Garolera, D., López, C.M., Carol I. & Papanastasiou, P. 2005. Micromechanical analysis of the rock sanding problem. *Journal of the Mechanical Behaviour of Materials*, 13, (1-2): 45-53.
- Ingraffea, A. R. & Saouma, V. E. 1985. Numerical modelling of discrete crack propagation in reinforced and plain concrete. In *Fracture Mechanics of concrete*, G. Sih and A. Di Tomasso, (Eds.), pp. 171-225. Martinus Nijhoff, Dordrecht, The Netherlands.
- Kupfer, H., Hilsdorf, H. & Rüschi, H. 1969. Behavior of concrete under biaxial stresses, *J. Am. Concrete Inst.* 66: 656–666.
- Lilliu G. & van Mier J.G.M. 2003. 3D lattice type fracture model for concrete. *Engineering Fracture Mechanics* 70(7/8): 927-941.
- Lopez, C.M. 1999. *Microstructural analysis of concrete fracture using interface elements. Application to various concretes* (In Spanish). Doctoral Thesis. ETSECCCPB, UPC, Barcelona. Spain.
- López, C., Carol, I. & Aguado, A. 2000. Microstructural analysis of concrete fracture using interface elements, *ECCOMAS2000*, Barcelona, Spain, CIMNE.
- Lopez, C.M., Carol, I. & Murcia, J. 2001. Mesostructural modeling of basic creep at various stress levels. *Creep, Shrinkage and Durability Mechanics of Concrete and other Quasi-Brittle materials*, Elsevier Publishers. Oxford, pp 101-106.
- Lopez, C.M., Ciancio, D. & Carol, I. 2004. Effect of interface dilatancy and specimen size in meso-mechanical analysis of concrete. In C.A. Mota Soares, et al., editor, *Metodos Computacionais in Engenharia - (Proc. of the Int. Conf. in Lisbon 31/May 2/Jun)*. APMTAC–SEMNI. In CD-ROM, ISBN 972-49-2008-9.
- Lopez, C.M., Segura, J.M., Idiart, A.E. & Carol, I. 2005a. Mesomechanical Modeling of Drying Shrinkage Using Interface Elements, *Creep, Shrinkage and Durability of Concrete and Concrete Structures*. Concreep 7, G. Pijaudier-Cabot, B. Gérard, P. Acker, eds. Nantes, France, 107-112.
- Lopez, C.M., Idiart, A.E. & Carol, I. 2005b. Mesomechanical analysis of concrete deterioration including time dependence, *Computational Plasticity VIII (COMPLAS 8)*, DRJ, Owen, E. Oñate, B. Suarez, eds. CIMNE (Barcelona, Spain) pp. 1059-1062.
- Norling, K. 1994. *Self-desiccation in concrete*, Licenciante Thesis, Chalmers University of Technology, Goteborg, Sweden.
- Okabe, A., Boots, B. & Sugihara K., 1992. *Spatial tessellations: concepts and applications of Voronoi diagrams*, John Wiley & Sons.
- Prat, P., Gens, A., Carol, I., Ledesma, A. & Gili, J. 1993. DRAC: A computer software for the analysis of rock mechanics problems. In H. Liu, editor, *Application of computer methods in rock mechanics*, 2, pp. 1361-1368, Xian, China. Shaanxi Science and Technology Press.
- Ribó, R. & Riera, M. 1997. Gid, the personal pre and post processor. Technical report, CIMNE-UPC-Barcelona, Spain.
- Roa, O., López, C.M., Pisoni, P., Pini, M., Carol, I. & Contro, R. 2000. Microstructural analysis of cancellous bone taking into account geometrically non-linear effects. *ECCOMAS 2000*, Barcelona, Spain, CIMNE.
- Roa, O. 2004. *Análisis microestructural del comportamiento mecánico del hueso trabecular* (In Spanish). Doctoral Thesis. ETSECCCPB, UPC, Barcelona. Spain.
- Roelfstra P.E., Sadouki H. & Wittmann, F.H. 1985. Le beton numerique. *Materials and Structures* 18 309-317.
- Rots, J. G. 1988. *Computational modelling of concrete fracture*. PhD thesis, Delft University of Technology, Delft, The Netherlands.
- Schlangen E. & van Mier J.G.M. 1993. Lattice model for simulating fracture of concrete. In F. H. Wittmann (Ed.), *Numerical Models in Fracture Mechanics of Concrete*. Balkema, Rotterdam, pp.195-205, (1993).
- Stankowski T. 1990. *Numerical simulation of progressive failure in particle composites*. Doctoral Thesis, Dept. CEAE, University of Colorado, Boulder, CO 80309-0428, USA.
- van Mier, J. 1997. *Fracture Processes of Concrete*. CRC Press.
- Vonk R. 1992. *Softening of concrete loaded in compression*. PhD thesis, Technische Universiteit Eindhoven, Postbus 513, 5600 MB Eindhoven, The Netherlands.
- Wang, J. & Huet, C. 1993. A numerical model for studying the influences of pre-existing microcracks and granular character on the fracture of concrete materials and structures. In C. Huet (Ed.) *Micromechanics of Concrete and Cementitious Composites*, Presses Polytechniques et Universitaires Romandes, Lausanne, Suiza, pp. 229.
- Willam, K., Pramono, E. & Sture, S. 1987. Fundamental issues of smeared crack models. In S. Shah, and S. Swartz, (Eds.), *Proc SEM-RILEM Int. Conf. on Fracture of Concrete and Rock*, SEM, Bethel., pp. 192-207